LA-UR 89-430

(2)

Los Alamos National Laboratory is operated by the University of California for the United States Department of Energy under contract W-7405-ENG-36

TITLE EARLY TIME DEBRIS STRUCTURING DUE TO THE ION-ION FILAMENTATION INSTABILITY

AUTHOR(S) V. A. Thomas, X-1
D. Winske, X-1

SUBMITTED TO Report prepared for the Defense Nuclear Agency

Los Alamos Los Alamos National Laboratory
Los Alamos, New Mexico 87545

AD-A205 722

REPORT DOCUMENTATION PAGE

1a. REPORT SECURITY CLASSIFICATION: UNCLASSIFIED	1b. RESTRICTIVE MARKINGS
2a. SECURITY CLASSIFICATION AUTHORITY	3. DISTRIBUTION / AVAILABILITY OF REPORT: Approved for public release
2b. DECLASSIFICATION / DOWNGRADING SCHEDULE	
4. PERFORMING ORGANIZATION REPORT NUMBER(S)	5. MONITORING ORGANIZATION REPORT NUMBER(S)
6a. NAME OF PERFORMING ORGANIZATION: Los Alamos National Lab. / 6b. OFFICE SYMBOL (If applicable): X-1	7a. NAME OF MONITORING ORGANIZATION
6c. ADDRESS (City, State, and ZIP Code): Los Alamos, New Mexico 87545	7b. ADDRESS (City, State, and ZIP Code)
8a. NAME OF FUNDING / SPONSORING ORGANIZATION: Defense Nuclear Agency / 8b. OFFICE SYMBOL (If applicable): RAAE	9. PROCUREMENT INSTRUMENT IDENTIFICATION NUMBER
8c. ADDRESS (City, State, and ZIP Code): Washington DC 20305	10. SOURCE OF FUNDING NUMBERS: PROGRAM ELEMENT NO. / PROJECT NO. RB / TASK NO. RC / WORK UNIT ACCESSION NO. 167

11. TITLE (Include Security Classification)
EARLY TIME DEBRIS STRUCTURING DUE TO THE ION-ION FILAMENTATION INSTABILITY (U)

12. PERSONAL AUTHOR(S)
V. A. Thomas and D. Winske

13a. TYPE OF REPORT	13b. TIME COVERED	14. DATE OF REPORT (Year, Month, Day)	15. PAGE COUNT
Technical	FROM 9/88 TO 2/89	89 Febr. 1	27

16. SUPPLEMENTARY NOTATION
This work was sponsored by the Defense Nuclear Agency under Project Code RB, Task Code RC, Work Unit No. 167, Work Unit Title "Simulations and Modeling of HANE/VHANE"

17 COSATI CODES		
FIELD	GROUP	SUB-GROUP

18. SUBJECT TERMS (Continue on reverse if necessary and identify by block number)
Early time structuring, Numerical simulations, Plasma instabilities

19. ABSTRACT (Continue on reverse if necessary and identify by block number)

Linear theory shows that when a plasma is created with a drift relative to an ambient plasma across a magnetic field, a robust electromagnetic instability is excited, if the drift speed exceeds the local Alfven velocity $V_0 > V_A$. Simulations of this ion-ion filamentation instability in a homogeneous system show that large amplitude waves with $\delta B/B_0 > 1$ develop nonlinearly, giving rise to large density clumping due to the non gyrotropic nature of the ion velocity distribution. In this report hybrid simulations are performed to examine the consequences of the ion-ion filamentation instability for H.A.N.E. applications. Uniform periodic simulations are considered as well as simulations consisting of a finite sized debris plasma interacting with a background plasma. In the later case the filamentation instability can be examined in the realistic situation where a high Mach number collisionless shock is generated. Of particular interest is whether the ion-ion filamentation instability forms long lasting structure (on a time scale greater than the shock formation time) in the debris piston. The simulations indicate that large amplitude density perturbations with $\delta n_D \gg n_A$ (D represents the debris plasma and A represents the air) generated by the ion-ion filamentation instability at early time do persist in the piston, especially at the debris-air interface. The filamentation instability may be responsible for some of the debris and background plasma structure associated with a H.A.N.E., although separating out effects due to other instabilities, such as the Alfven ion cyclotron instability, is most difficult.

20. DISTRIBUTION / AVAILABILITY OF ABSTRACT	21. ABSTRACT SECURITY CLASSIFICATION
☒ UNCLASSIFIED/UNLIMITED ☐ SAME AS RPT. ☐ DTIC USERS	UNCLASSIFIED
22a. NAME OF RESPONSIBLE INDIVIDUAL: Dr. Vincent A. Thomas	22b. TELEPHONE (Include Area Code): 505-665-0796 / 22c. OFFICE SYMBOL: X-1

DD FORM 1473, 84 MAR — 83 APR edition may be used until exhausted. All other editions are obsolete.

Early Time Debris Structuring due to the Ion-Ion Filamentation Instability

V. A. Thomas and D. Winske
Applied Theoretical Physics Division
Los Alamos National Laboratory
Los Alamos, NM 87545

February 1, 1989

Abstract

Linear theory shows that when a plasma is created with a drift relative to an ambient plasma across a magnetic field, a robust electromagnetic instability is excited, if the drift speed exceeds the local Alfven velocity $V_0 > V_A$. Simulations of this ion-ion filamentation instability in a homogeneous system show that large amplitude waves with $\delta B/B_0 > 1$ develop nonlinearly, giving rise to large density clumping due to the non gyrotropic nature of the ion velocity distribution. In this report hybrid simulations are performed to examine the consequences of the ion-ion filamentation instability for H.A.N.E. applications. Uniform periodic simulations are considered as well as simulations consisting of a finite sized debris plasma interacting with a background plasma. In the later case the filamentation instability can be examined in the realistic situation where a high Mach number collisionless shock is generated. Of particular interest is whether the ion-ion filamentation instability forms long lasting structure (on a time scale greater than the shock formation time) in the debris piston. The simulations indicate that large amplitude density perturbations with $\delta n_D \gg n_A$ (D represents the debris plasma and A represents the air) generated by the ion-ion filamentation instability at early time do persist in the piston, especially at the debris-air interface. The filamentation instability may be responsible for some of the debris and background plasma structure associated with a H.A.N.E., although separating out effects due to other instabilities, such as the Alfven ion cyclotron instability, is most difficult.

I. Introduction

The late time plasma structure resulting from a H.A.N.E. can be detrimental to communications and sensors of various kinds. In this regard it is important to be able to characterize the scale sizes of the density fluctuations ('structure") in the late time limit. However, in order to do this it is necessary to know the process involved in the structure formation. The question arises as to whether the late time structure is related only to processes that occur late in time or whether the early time behavior of the initial debris/air interaction plays a part in determining the late time plasma characteristics. Recently, work at Austin Research Associates [Thompson *et al.*, 1988] has focused attention on the ion-ion filamentation instability (hereafter sometimes referred to as the IIF instability) as an early time candidate which may be important for determining late time plasma structure.

The purpose of this report is to examine the ion-ion filamentation instability using hybrid particle simulations. It is important to keep in mind that the ion-ion filamentation instability is closely related to the Alfven ion cyclotron (AIC) instability [Davidson and Ogden, 1975, Tanaka *et al.*, 1983, Tanaka *et al.* 1985; Ambrosiano and Brecht, 1987; Otani, 1988; and references therein], an instability that has been extensively studied using both theory and simulations. The free energy for both instabilities is an anisotropy in the ion energy with $E_{i\perp}/E_{i\|} > 1$ where $\perp$ ($\|$) is the direction perpendicular (parallel) to the ambient magnetic field. The linear theory for these instabilities will be briefly reviewed in Section 2. Previous simulations of the ion-ion filamentation instability [Thompson *et al.*, 1988] and the Alfven ion cyclotron instability [Ambosiano and Brecht, 1987] in a homogeneous system show that large amplitude waves with $\delta B/B_0 > 1$ develop for both instabilities. Large density clumping only occurs for the filamentation instability due to the nongyrotropic nature of the ion distribution function. Previous simulations of the AIC instability in a shock environment showed the development of both large amplitude waves with $\delta B/B_0 > 1$ and density perturbations with $\delta n/n_0 > 1$ [Thomas and Brecht, 1986; Winske and Quest 1988]. No simulations to look specifically for the ion-ion filamentation instability in a shock environment have been carried out. Later, we will comment on why it was not observed in previous simulations where it might have been excited.

This report addresses the behavior of the ion-ion filamentation instability in a uniform system, and more relevant to the H.A.N.E. problem, its evolution in a situation where a high Mach number shock is generated. As in homogeneous configurations, the shock simulations show that large amplitude density fluctuations are produced in both plasma species. This structure persists even when the shock front is considerably ahead of the debris piston, suggesting that the ion-ion filamentation may be responsible for some of the ionized structure associated with a H.A.N.E. in both the debris and the background plasma which remains behind the front of the debris piston. However, as will be shown later, distinguishing structure produced by the IIF from that associated with the AIC is very difficult.

The rest of the report includes a brief review of linear theory, a short description of the simulation model, and a discussion of the simulation results for the ion-ion filamentation instability in both homogeneous systems and in a shock environment. The final section will list the salient results and outstanding questions.

II. Linear Theory

Linear theory for the AIC instability is well described in Davidson and Ogden [1975] and Ambrosiano and Brecht [1987], while properties of the IIF instability are worked out in Thompson *et al.* [1988]. As we shall show, for the most unstable case, namely for $\vec{k}$ parallel to $\vec{B}$, the two modes are essentially equivalent.

For $\vec{k} \parallel \vec{B}$, the linear dispersion equation for transverse electromagnetic waves is

$$\omega^2 - c^2k^2 - \sum \omega_j^2 + \sum \frac{\omega_j^2}{2} \int d^3v \frac{kv_\perp^2 \partial F_j/\partial v_\parallel \pm 2\Omega_j F_j}{\omega - kv_\parallel \pm \Omega_j} = 0 \qquad (1)$$

where F_j, $\omega_j = (4\pi e_j^2 n_j/m_j)^{1/2}$, and $\Omega_j = e_j B_o/m_j c$ are the velocity distribution function, the plasma frequency, and the cyclotron frequency for the j-th species of mass m_j, charge e_j, and density n_j. Assuming F_j can be factored into a $v_\perp$ part and a Maxwellian $v_\parallel$ part (with thermal speed v_j), (1) can be written as

$$\omega^2 - c^2k^2 - \sum \omega_j^2 + \sum \frac{\omega_j^2}{2}(1 - \frac{T_{\perp j}}{T_{\parallel j}})Z' \pm \sum \omega_j^2 \frac{\Omega_j}{kv_j} Z \; = \; 0 \qquad (2)$$

where the argument of the plasma dispersion function (Z) is $(\omega \pm \Omega_j)/kv_j$ and $T_{\parallel j} = \frac{1}{2}m_j v_j^2$ and $T_{\perp j} = \int \frac{1}{2} m_j v_\perp^2 F_{\perp j} d^2v$. Thus, whether the perpendicular distribution is a Maxwellian $F_{\perp j} \sim \exp(-v_\perp^2/v_{\perp j}^2)$, a ring distribution, $F_{\perp j} \sim \delta(v_\perp - V_r)$ or a beam, $F_{\perp j} \sim \delta(v_{\perp 1})\delta(v_{\perp 2} - V_b)$, does not matter when $\vec{k} \parallel \vec{B}$ (the most unstable case): the perpendicular velocity distribution enters only through the second velocity moment, "$T_\perp$". It should also be noted that the basic instability mechanism does not depend on whether the driving anisotropy $T_\perp/T_\parallel$ is in the ions or the electrons, or even if there is an ambient magnetic field present. (Hereafter, we shall use $T_\perp/T_\parallel$ to mean $T_{i\perp}/T_{i\parallel}$.) Under different conditions, the instability has been called various names (e.g., electron Weibel, electron whistler, ion Weibel, ion whistler, electromagnetic ion cyclotron, Alfven ion cyclotron, etc.). It has been extensively studied theoretically and is a favorite mode for testing electromagnetic simulations codes [e.g., Morse and Nielson, 1971; Brackbill and Forslund, 1982; Otani, 1988].

However, we will specialize to the H.A.N.E. case and consider debris ions streaming relative to the air across a magnetic field B_o, as depicted in Figure 1. We know this

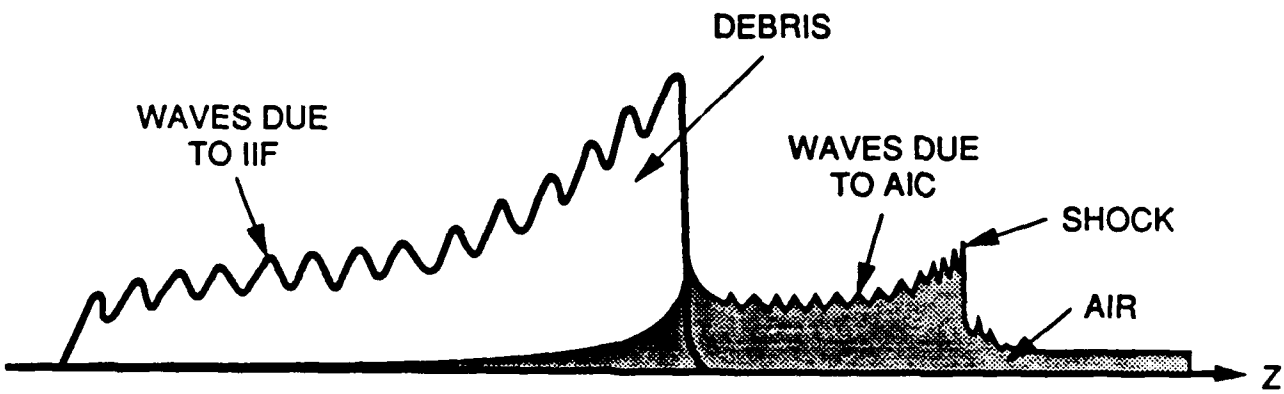

Figure 1. Schematic of the simulations showing the ion-ion filamentation instability (IIF) developing in the debris and the Alfven ion cyclotron instability (AIC) at the shock front.

situation can be unstable to various fast growing, electrostatic instabilities [Lampe *et al.*, 1975], but when the debris velocity exceeds the Alfven speed, they are either stable or not very efficient at coupling the streams together. Instead, a collisionless shock forms in front of the debris [e.g., Thomas and Brecht, 1986]. Because the Mach number ≥ 3, the shock reflects ions and the AIC instability is excited as the reflected ions form a ring distribution at the shock front, giving rise to $T_\perp/T_\parallel \gg 1$ [Wu *et al.*, 1984]. However, Thompson *et al.* [1988] have shown that for the debris streaming relative to the air, the ion-ion filamentation instability can also be excited with a very large growth rate, $\gamma \gg \Omega_i$. Because it does not give rise to momentum coupling (the wavevectors are primarily along $\vec{B}$, not the streaming direction), it has not been given serious attention in the past. As we have previously discussed, these two instabilities are not separate entities, but as their sources of free energy are different, we shall treat them as such in the subsequent discussion. In fact, in the Appendix we show that the two instabilities are practically indistinguishable, as will be apparent in the simulations to follow.

We briefly review two interesting aspects of these instabilities. First, we consider their linear properties. Assuming for simplicity that the debris and air ions have the same density, mass, and $\beta_j = 8\pi n_j T_{\parallel j}/B_o^2 = 1$, we consider numerical solutions of (2) for different values of $T_\perp/T_\parallel = 4, 16, 36$. (For the IIF this corresponds to the ions having velocities $\pm V_b = 2, 4, 6 v_A$ (v_A =Alfven speed using the total ion density). Figure 2 shows growth rates normalized to Ω_A versus wavenumber kc/ω_A. For a given value of $T_\perp/T_\parallel$, the growth rate peaks for $kc/\omega_A \sim 1$, and falls to zero as $k \to 0$ and for k large. Decreasing $T_\perp/T_\parallel$ decreases the maximum growth rate and the range of wavenumbers over which the instability is excited (cf, Figure 2 of Davidson and Ogden, [1975]). Furthermore, it can be shown [Davidson and Ogden, 1975] that at maximum growth:

$$\frac{\gamma}{\Omega_i} \simeq (\frac{\beta_i}{2}\frac{T_\perp}{T_\parallel})^{1/2} \tag{3}$$

[cf Eq. (207) of Thompson *et al.*, (1988)] and for $\beta_i \simeq 1$,

$$\frac{kc}{\omega_i} \simeq \frac{3}{4}(\frac{T_\perp}{T_\parallel})^{1/2} \tag{4}$$

Second, we briefly recall the nonlinear properties of the instability. Consistent with both quasilinear theory and simulations, as the instability evolves, the growing unstable waves pitch angle scatter the ions. This reduces the anisotropy and shifts the dominant wavenumber for growth to smaller values (cf, Figure 2). Lemons *et al.* [1979] show from a general thermodynamic argument for the analogous electron instability that the maximum magnetic field fluctuations, δB^2, are given in terms of the initial parameters:

$$\frac{\delta B}{B_o} \simeq (\frac{1}{12}\beta_i\frac{T_\perp}{T_\parallel})^{1/2}(1 - \frac{T_\parallel}{T_\perp})^2 \tag{5}$$

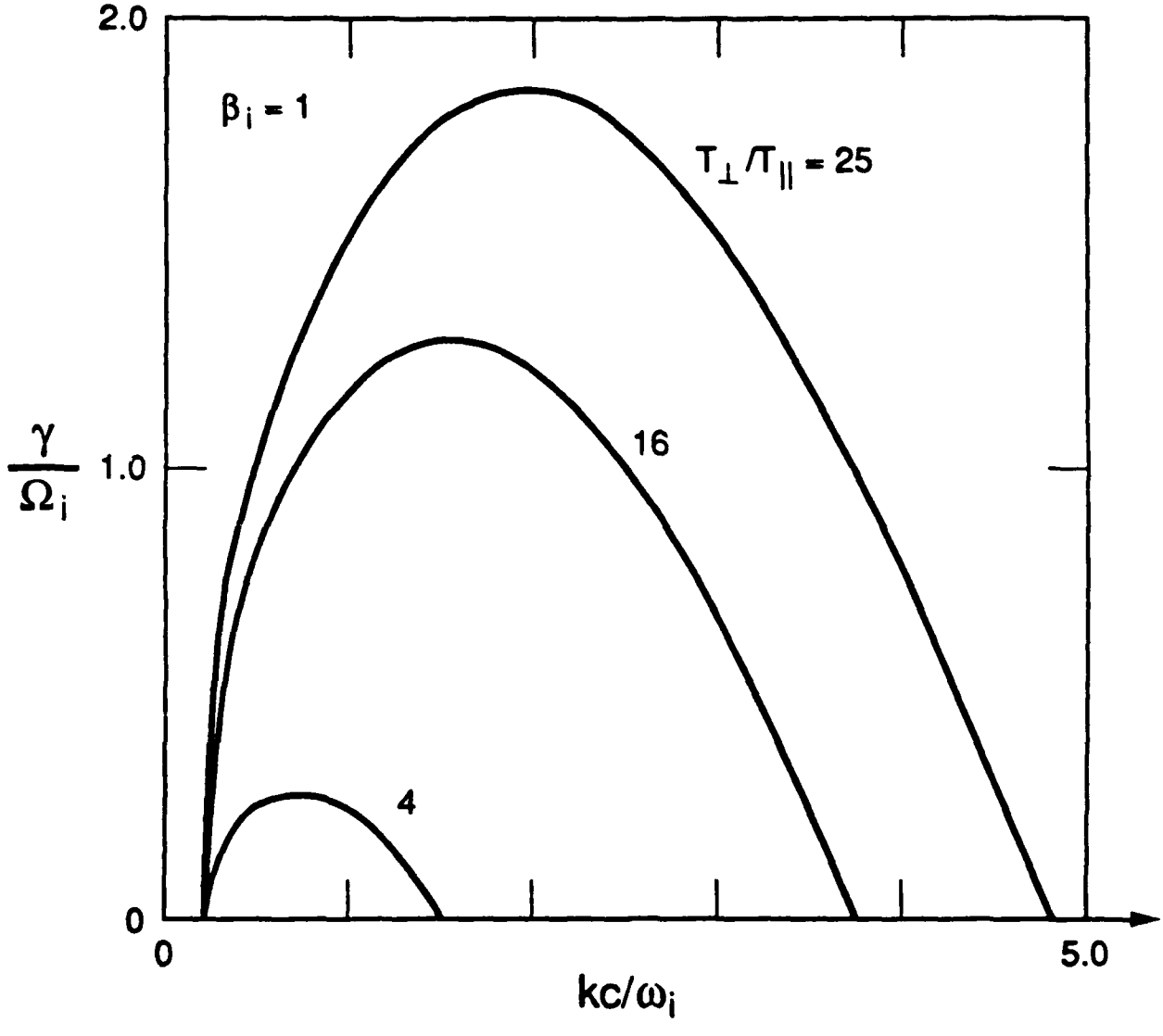

Figure 2. Numerical solutions of (2) for the ion-ion filamentation instability for V_b/v_A =2,3, and 4; equivalently for the Alfven ion cyclotron instability with $T_\perp/T_{||} = 4, 16, 25$ ($\beta_i = 1$) showing growth rates γ/Ω_i versus wavenumber, kc/ω_i.

which is well confirmed in the simulations of Ambrosiano and Brecht [1987] (Figure 7) and those to follow in this report. The theory also predicts that a residual anisotropy will remain in a system of finite length L, where $k_f = 2\pi/L$ and

$$(\frac{T_\perp}{T_\parallel})_f \simeq 1 + (\frac{k_f c}{\omega_i})^2 \tag{6}$$

III. Simulations

A. Preliminaries

The simulation model uses massless fluid electrons and particle ions, assumes quasineutrality and ignores the transverse component of the displacement current. Thus, the model retains the physics necessary to describe low frequency electromagnetic phenomena together with ion kinetic effects [Brecht and Thomas, 1988]. The simulations described in this paper use an algorithm for solving the electromagnetic field equations given in Quest [1988]. Similar simulations have also been performed using the predictor-corrector method of Harned [1982]. The results obtained are substantially independent of the field algorithm used.

A variety of simulations have been performed, including 1-D and 2-D simulations of a periodic homogeneous system, and 2-D simulations appropriate for the generation of a shock wave for H.A.N.E. initial conditions. Many parameters were varied including the ratio of the debris plasma to the background plasma, the thermal speeds of the various components, the lengths of the simulation region, and the use of different initial conditions for generation of the instability in a shock environment. We show only very few of the results, just enough to emphasize the most important points.

For the homogeneous runs the magnetic field is along the z direction, the simulation coordinate for the 1-D runs. The 2-D runs are in the z-x plane. The initial debris beam velocity is along x, with the background ions at rest. The density ratio is $n_D/n_A = 9$. The system length is calculated in terms of c/ω_i, where the total ion density is used to calculate the ion plasma frequency. Both species have the same mass and initially are cold, with essentially no thermal velocity. Typically, 50-100 cells are used in the 1-D runs, with 10000 simulation particles; a 50 × 50 grid is used for the 2-D cases (e.g., Case 6) with 200,000 particles. As shown in Table 1, typical cell sizes range from 0.2 -0.5 c/ω_i with time steps of $\Omega_i \Delta t \sim 0.01$.

Filamentation Simulations							
case	type	$L_z(n_z)$	$L_x(n_x)$	$\beta_\perp$	$T_{i\perp}/T_{i\parallel}$	$\delta B/B_0$	$\delta n/n_0$
1	1-DP	10(50)		9.0	10^6 21	1.6	4.4
2	1-DP	25(50)		9.0	10^6 10	2.6	3.9
3	1-DP	50(100)		9.0	10^6 3.6	3.3	3.7
4	1-DP	50(100)		9.0	30 2	1.5	1.6
5	1-DP	15.8(50)		90	200 3.8	8.7	2.8
6	2-DP	15.8(50)	158(50)	90	200 2.5	20	2.8
7	2-NDP	100(200)	5(50)			15	5.2
8	2-NDP	100(200)	5(50)			15	2.4

Table 1. List of some of the simulations indicating the simulation parameters and results. Cases 1-5 are one dimensional periodic simulations, case 6 is a two dimensional periodic simulation, and cases 7 and 8 are two dimensional nonperiodic simulations. Cases 1-3 are initialized with a finite perturbations in mode three of the system, making the runs essentially single mode simulations. The other simulations were initialized with random perturbations. The density ratio of the debris to the background plasma was 9 for the periodic runs. Case 7 has a nonuniform debris piston with a maximum ratio of 9 to 1 relative to the background plasma (45 to 1 in Case 8). The lengths are expressed in terms of c/ω_{pi} calculated using the total ion density except for cases 7 and 8, which are calculated in terms of the background ion density. The numbers in parentheses indicate the number of simulation cells used. The ambient magnetic field is in the z direction for all cases except for cases 7 and 8, where it is in the x direction. The initial streaming direction is in the x direction for all simulations except for cases 7 and 8, where it is in the z direction. $\beta_\perp$ is the initial perpendicular thermal beta of the plasma. The first entry in the temperature ratio column gives the initial temperature anisotropy whereas the second entry gives the calculated anisotropy at the end of the simulation. $\delta B/B_0$ and $\delta n/n_0$ are the peak fluctuations in the magnetic field strength and total plasma density as observed in the simulation. ($n_0$represents the maximum initial plasma density). The values of these fluctuations at the end of the simulations is somewhat reduced.

For the inhomogeneous runs in two dimensions a debris slug of parabolic shape in the streaming (z) direction with thickness L_D and uniform in the direction (x) along the ambient magnetic field interacts with a uniform air background. The maximum debris density relative to the air is nine, and quantities are normalized in terms of the air parameters. The initial streaming velocity of the debris relative to the air is $10v_A$, where the Alfven speed is computed using the air density. For the two runs to be shown later, 300,000 simulation particles were employed with the system size of $100 \times 5c/\omega_i$ with $\Delta z = 0.5c\omega_i$ and $\Delta x = 0.1c/\omega_i$ (to emphasize the short wavelengths that are excited along x) and $\Omega_i \Delta t = 0.14$.

B. Periodic Simulations

In this section we describe the periodic simulations, which were carried out in order to examine the linear and nonlinear properties of the ion-ion filamentation instability in a homogeneous system. We have varied the system length, the ratio of the debris plasma to the background plasma, the thermal speeds of the plasmas, and whether the system is 1-D or 2-D. Table 1 summarizes the simulation parameters and some results of the various cases run. A few salient features of the results are shown in Figures 3-7.

Figure 3 shows time histories of the fluctuating magnetic field energy and the debris and background ion kinetic energy for cases 1-4. All four cases have the same $\beta_{i\perp} = 9$. In the first three cases $T_{i\perp}/T_{i\parallel}$ is essentially infinite. In each case the simulation is initialized with a perturbation in mode m=3, which corresponds to a different wavelength as the system size is changed in each case. The magnetic field fluctuation energy histories in all four cases show intervals where the growth is exponential. The measured growth rates of the first two cases are nearly identical ($\gamma/\Omega_i = 2.2 \pm 0.2$ and 1.9 ± 0.1) consistent with (3), i.e., the maximum growth rate depends only on $\beta_{i\perp}$. Consistent with (4), the mode with the largest growth rate is actually shorter than those imposed in these cases. Similarly, one sees from Figure 3 the reduction in the growth rate of cases 3 ($\gamma/\Omega_i \simeq 1.4 \pm 0.1$) and 4 ($\gamma/\Omega_i \simeq 0.12 \pm 0.02$) as the unstable wave is made longer (case 3) and as the initial anisotropy (case 4) is reduced is evident, again pointing out the limited usefulness of (3) and (4). A numerical solution of (2) yields growth rates for the four cases ($\gamma/\Omega_i = 1.7, 1.1, 0.6, 0.4$), which are in fair agreement with the simulations. A difficulty with comparing linear theory to the simulations stems from the fact that the theory assumes the calculation is done in the center of mass frame, whereas the simulations are done in the rest frame of the air ions, in order to compare the results with the inhomogeneous simulations to be described later. Further, it is evident from Table 1 (righthand side of column 6) that when only shorter wavelengths are allowed in the system (by reducing the system length), the final ion temperature anisotropy is much larger than if longer wavelengths are also allowed. This is true even though the maximum perturbations in the field and density are only weakly dependent upon the system lengths, and is consistent with the (6). Also seen in Table 1 from the small values of $\delta B/B_0$ and $\delta n/n_0$ is the quenching effect that smaller initial ion

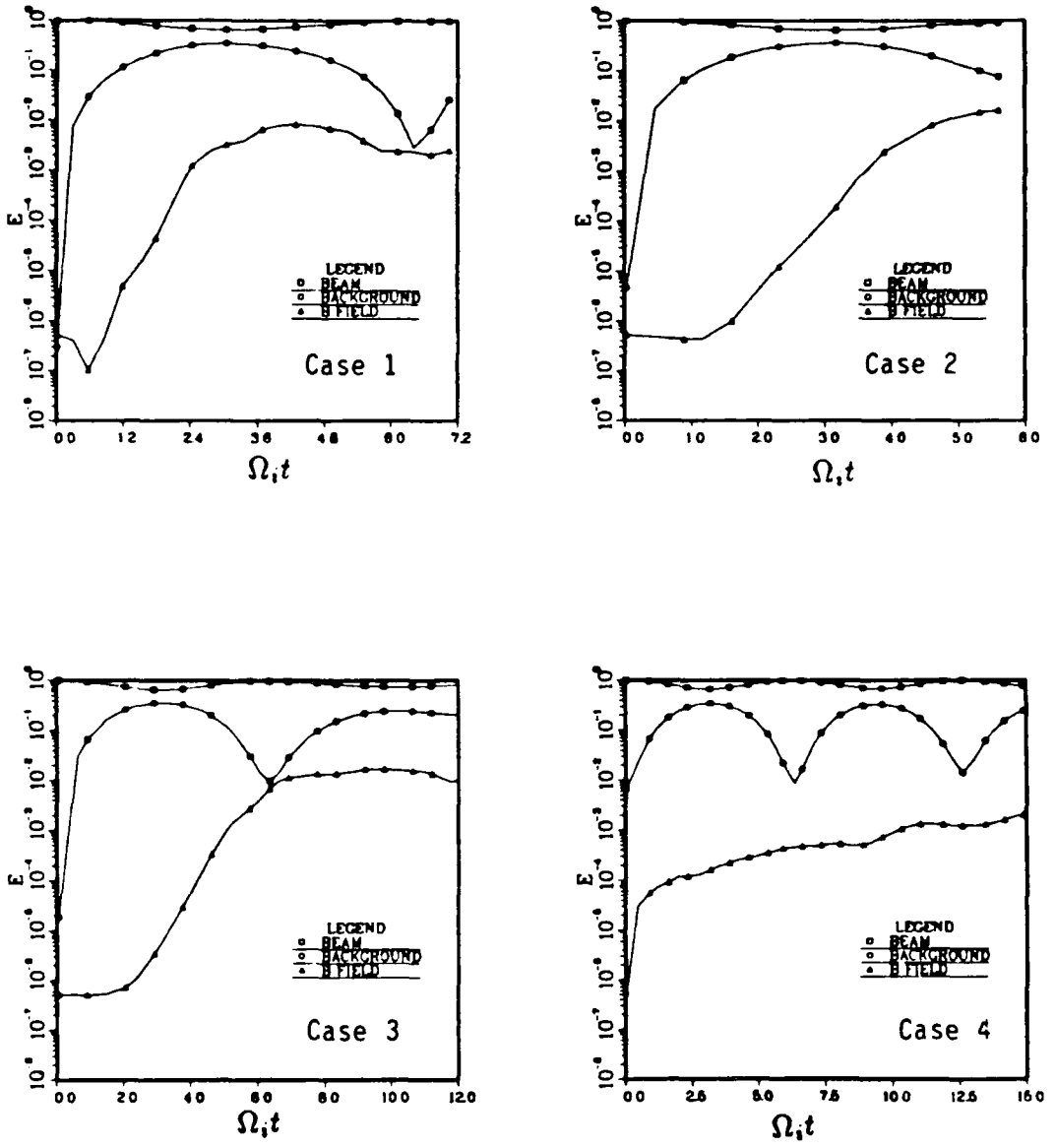

Figure 3. Energy partition as a function of time. Exponential growth in the magnetic field energy occurs for cases (1) (2) and (3). Case (4) does not have exponential growth because the growth rate is smaller than the gyrofrequency and the mode polarization is changing quickly as a function of time. Debris (beam) and air (background) energies change out of phase due to gyromotion.

temperature anisotropies have on the instability, consistent with (5). Also shown in Figure 3 are the time histories of the kinetic energies for both ion species, denoted in the figure as the beam (i.e., debris) and background (air). The energies of both ion components oscillate with a period of $2\pi/\Omega_i$, which evidently corresponds to gyromotion of the debris about the magnetic field and the out of phase response of the background plasma. The fact that the kinetic energies oscillate again points out that the instability does not give rise to much momentum or energy coupling of the two species.

Figures 4 and 5 show profiles in z of the transverse components of the magnetic field (B_y and B_x) as well as the magnitude of B, and the debris, air (n_D and n_A) and total ion density at two times ($\Omega_i t = 3.2$ and 4.9) for Case 2. This simulation, as well as cases 1 and 3, is essentially a single mode simulation in which mode 3 was initially excited with a finite amplitude, while the other modes were not. Growth of the instability is observed for times on the order of the ion cyclotron period, and the polarization of the magnetic field perturbation changes in time approximately in the same direction as the instantaneous relative streaming direction. In this case, B_x was initially perturbed, while in the left hand panel in Figure 4 B_y is dominant ($\Omega_i t = 3.2$) and at a later time B_x is again dominant ($\Omega_i t = 4.9$) [right hand panel]. Thompson *et al.* [1988] show the magnetic field will be polarized primarily in the relative streaming direction as long as $\gamma \gg \Omega_i$. However, since the debris ions are rotating in the magnetic field, the streaming direction and hence the sense of polarization change on a time scale comparable to Ω_i.

Nonlinearly, large amplitude density perturbations develop. Initially, the density fluctuations of the two ion species are out of phase, with each species occupying areas vacated by the other species, so that the total ion density is roughly constant in space ($\sum n_i$ =constant). This is expected for parallel propagating electromagnetic waves: the total density fluctuations are second order in the field perturbations. Later in time during the nonlinear stage, the total ion density also develops significant fluctuations so that $\delta n/n \sim \delta B/B$. As is evident from the figure, the density variations become so large that there are regions where the density of each species is essentially zero. Note that since this is an electromagnetic instability, such large density perturbations do not lead to saturation of the instability. Compared to cases shown later, both the magnetic field and density fluctuations exhibit a rather odd behavior. Instead of the more usual cascade to longer wavelengths (as discussed below), shorter waves appear later in time. This occurs because the simulation was initialized artificially with a perturbation of fixed wavelength (mode 3 in this case). Although this mode grows to large amplitude, shorter waves that grow faster are still excited. Before they are quenched by the reduction of the anisotropy, they grow large enough to contribute noticeably to the spectrum. The fact that these modes appear on the edges of the debris cavities may also suggest some sort of parametric decay process is occurring in this case.

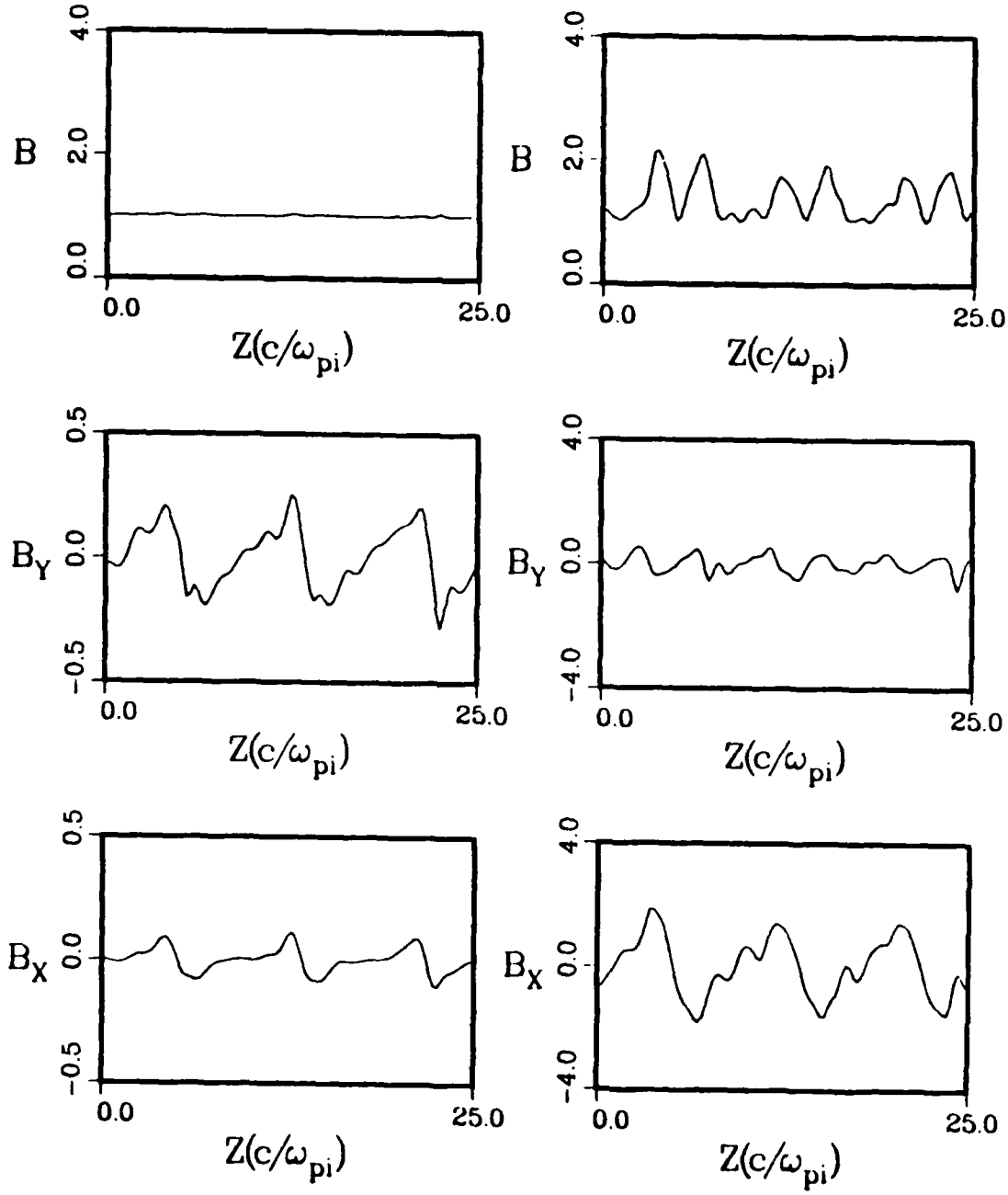

Figure 4. The magnetic field components B_z and B_y and the total magnetic field at $\Omega_i t = 3.2$ (left side) and$\Omega_i t = 4.9$ (right side) for case 2. Since the growth occurs over a time scale $\Omega_i t \sim \pi$, the dominant magnetic field component also changes in time. In this and all subsequent plots the magnetic field is normalized relative to the ambient magnetic field strength.

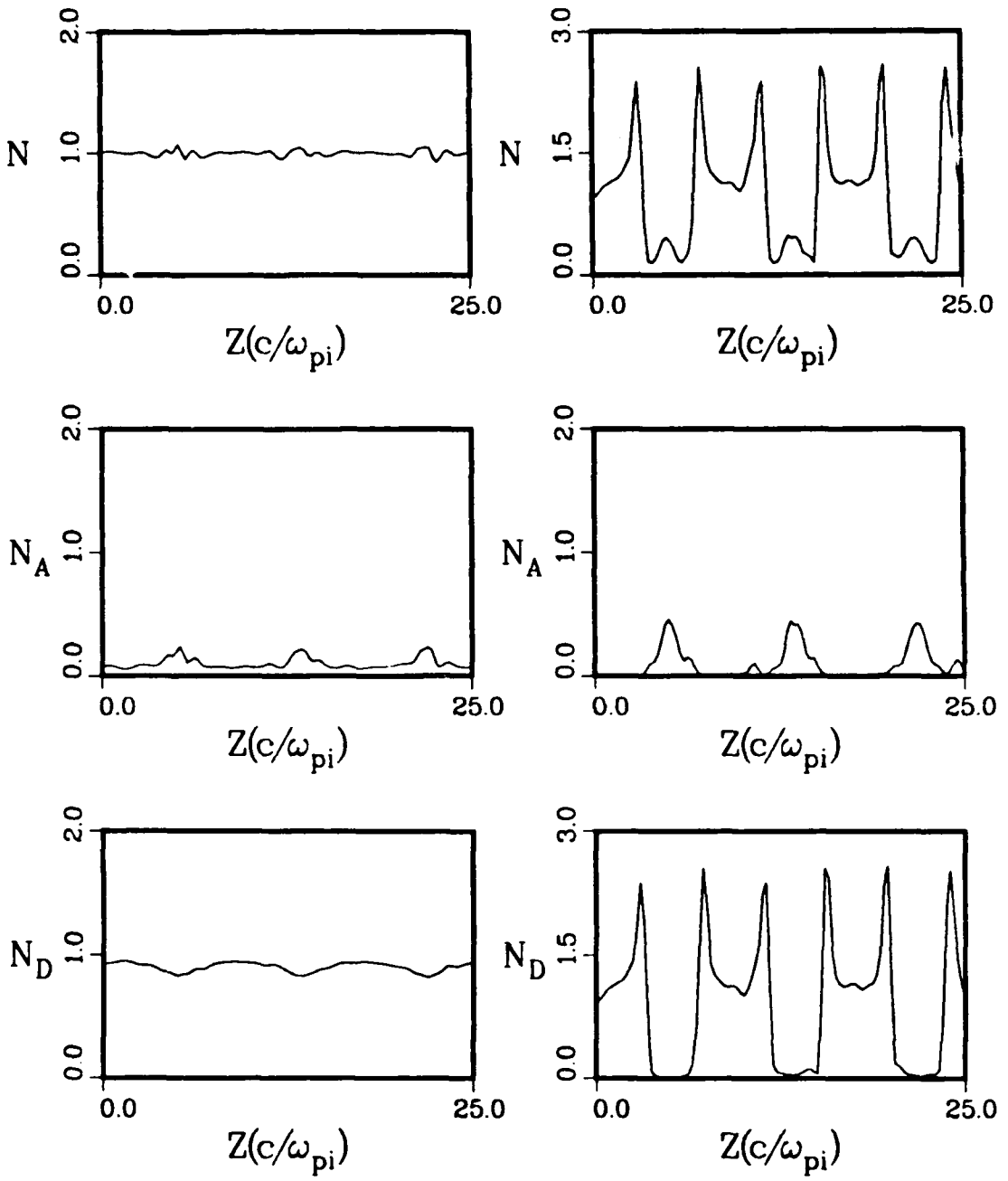

Figure 5. The debris density, the air density, and the total density corresponding to Figure 4. The two ion species tend to mutually exclude each other in space. In this and all subsequent plots the density is normalized relative to the total (debris plus background) initial density.

Case 5 displays the more common mode cascade from short wavelength to long wavelength perturbations. The simulation was initialized with random noise, so the fastest growing wavelength is very small due to the large ion temperature anisotropy, shorter than is resolvable by the simulation. Therefore, early in time the dominant wavelength is the shortest mode resolvable by the grid with a wavelength of approximately six or seven cells. The mode cascade is seen both in the plots of B_y and n_D in Figure 6. The presence of the mode cascade suggests that the short wavelength modes which grow early in time are irrelevant for the long time appearance of the nonlinear state. Thus, the physical mechanism controlling the short wavelength cutoff need not be known in order to understand the dominant long time, long wavelength state of the instability. The cascade to longer wavelengths has been seen in previous simulations of the filamentation instability [Thompson *et al.*, 1988] and the AIC instability [Ambrosiano and Brecht, 1987], and is a well known phenomena for such electromagnetic instabilities [Morse and Nielson, 1971]. The evolution of the instability is basically quasilinear. The shorter wavelength modes grow more rapidly, according to linear theory. This removes only a small portion of the anisotropy, leading to the stabilization of these modes and the continued growth of longer wavelength modes. The longest modes in the system remain unstable to infinitesimal ion temperature anisotropies [cf Eq. (6)]. Therefore, the long time behavior of the instability is dominated by wavelengths much longer than those corresponding to the fastest growing mode.

Finally, Figure 7 displays features of a two dimensional simulation corresponding to case 5, again showing B_y and n_D at three times. Note that in this case and those to follow that the scales change from panel to panel. There is a mode cascade, easier to see in the density than in B_y because of the change of the polarization of the wave discussed earlier. At the end of the simulation, the density perturbations are more aligned along the magnetic field. The maximum perturbation amplitudes are roughly the same as for the one dimensional simulation (Table 1), although the density depletions are not as evident in the figure. While structure exists across x, the dominant changes (cascade) occur along z. This is true because the maximum growth rates are for those modes with $k_\perp \ll k_\parallel$. In the homogeneous periodic model there is little difference induced by dimensional effects, i.e., by changing the size of L_x.

C. Inhomogeneous Simulations

In order to make the simulations more relevant to the H.A.N.E. case we consider the interaction of a finite debris piston with a uniform magnetized background plasma, similar to that of Thomas and Brecht [1986]. Two types of initial conditions have been examined. In one case the magnetic field is completely excluded from the debris piston; this is a good approximation for the early stages of an essentially collisionless H.A.N.E. Another type of initial condition is to assume that the ambient magnetic field is imbedded in the debris piston. This is not realistic for the early stages of a H.A.N.E. but it may be quite

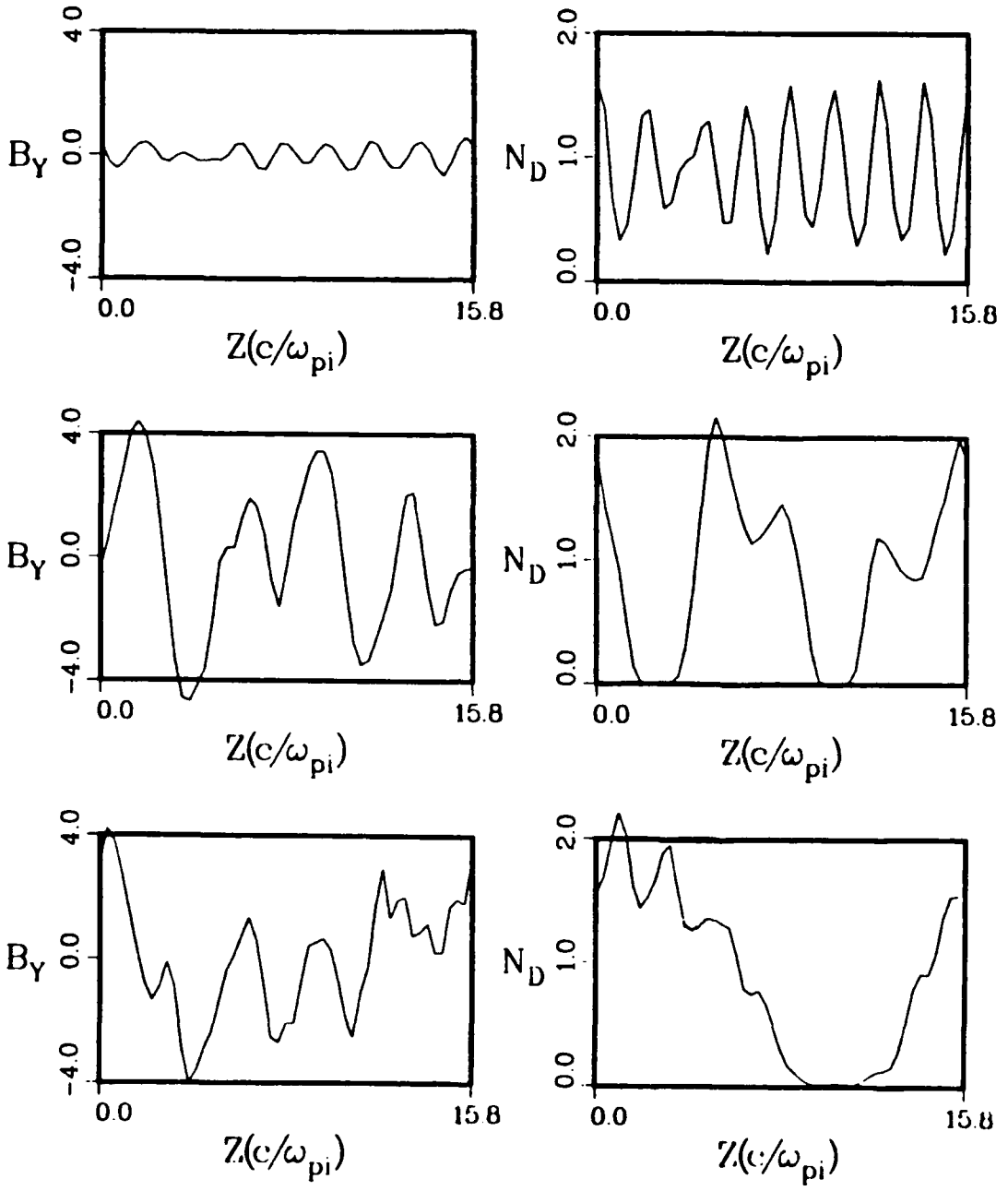

Figure 6. The magnetic field component B_y and the corresponding debris density at $\Omega_i t = 1.2, 3.5, 6.9$ for case 5. Time is increasing toward the bottom of the page. Late in time the longer wavelength perturbations dominate the system.

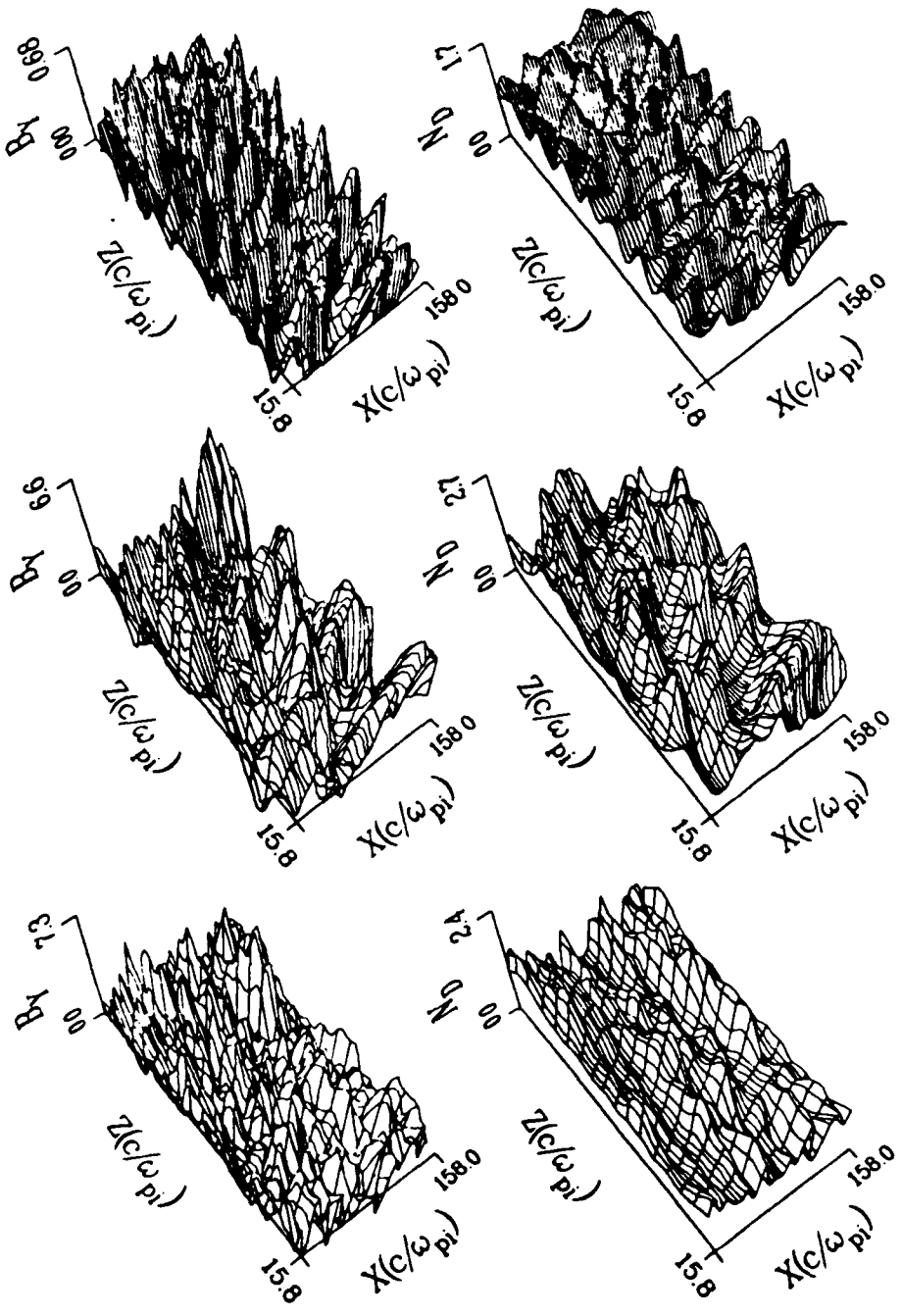

Figure 7. B_y and n_D corresponding to Figure 6. for a two dimensional periodic simulation with the same parameters as case 5. The results are qualitatively and quantitatively similar.

reasonable for the leading edge of the debris piston due to anomalous resistivity effects. There is relatively little difference in the results, since the dominant physics occurs at the interface between the debris piston and the background plasma. Thus, we will only show results for the case where the magnetic field is imbedded in the piston region initially. Figure 8 displays 3-D perspective plots of the debris ion density and the magnetic field component B_y for three times in the simulation of Case 7. At early time ($\Omega_i t = 0.6$) the ion-ion filamentation instability develops throughout the body of the piston; consistent with linear theory, waves grow on a time scale much faster than the ion gyroperiod and therefore much faster than the time for shock formation. Only small ripples can be seen in the debris density, but it is evident from the B_y plot that short wavelength fluctuations occur throughout the debris region. (The waves upstream in the air represent only noise.)

Later on ($\Omega_i t = 1.5$, still before shock formation), the waves continue to grow and on a time scale comparable to that of the homogeneous simulations, strong perturbations in the magnetic field and the density arise, particularly at the debris-air interface. The density and magnetic field perturbations are somewhat reduced from their values in the periodic homogeneous simulations in most of the interaction region, with the waves at the leading interface between the debris and the background plasma larger than in the homogeneous simulations. These differences are not a two dimensional effect, as we have seen that the two dimensional periodic simulations reveal similar perturbation amplitudes to the one dimensional periodic simulations. However, there are other possible contributing factors. First, the parameters of the interaction are comparable only for the peak in the debris shell, and not everywhere throughout the shell, leading to smaller perturbations in the interior of the debris shell. Second, the magnetic field is being swept up by the debris piston in these inhomogeneous simulations, which could compress and amplify the waves at the leading interface between the debris and the background and reduce the perturbations in the body of the debris shell. Third, the waves at the debris-air interface may be enhanced due to the strong gradients. Similar enhancements are seen at the ramp of high Mach number quasiperpendicular shocks [Thomas and Brecht, 1986; Winske and Quest, 1988] and are thought to be due to coupling to other modes, such as drift mirror and compressional drift waves. However, this enhancement may be an artifact of 2-D [Thomas, 1989]. Again, we note that on this short time scale ($\Omega_i t \sim 2$), little momentum and energy is exchanged between the two species.

In order to tranfer momentum and energy from the debris to the air, a shock wave forms out in front of the debris piston, as is seen in the bottom panels ($\Omega_i t = 4.3$). At the front of this collisionless shock wave are large amplitude magnetic and density perturbations produced from the AIC instability, as discussed previously by Thomas and Brecht [1986] and Winske and Quest [1988]. Although the calculation has not been carried out very far, it appears that the shock is unaffected by the development of structure in the debris piston. The largest amplitude perturbations are maintained at the interface between the debris piston and the background plasma, which is now somewhat removed from the shock front. Note that the maximum value of the debris density is greater than

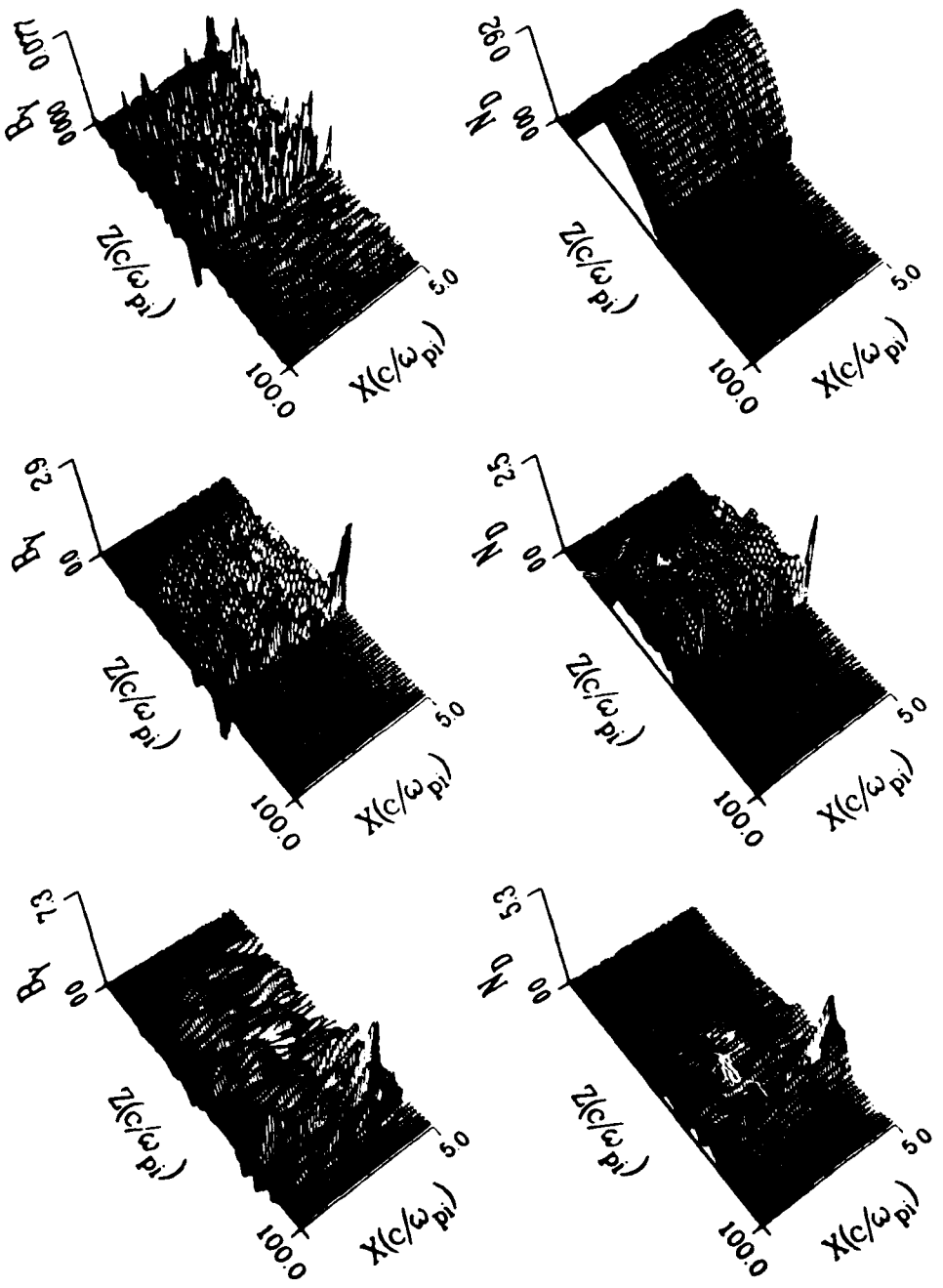

Figure 8. Three-dimensional perspective plots of B_y and n_D at $\Omega_i t = 0.6, 1.5, 4.3$ for a nonperiodic simulation with parameters corresponding to Figures 6-7 and debris thickness $L_D = 50c/\omega_i$. Early in time the magnetic field is polarized in the direction of relative streaming. Due to gyromotion, the B_y component quickly becomes comparable. Late in time the largest magnetic field perturbations are at the shock front of the shocked background plasma, while the density perturbations are largest at the debris-air interface.

5, while the initial debris density is 0.9 and the air density is 0.1. Thus, δn_D is greater than 5 times the initial debris density and more than 50 times the air density. And as in the homogeneous simulations, $\delta n/n \sim \delta B/B \gg 1$.

At this time the mode cascade to longer wavelengths (in x) can be seen in the body of the debris plasma, again in general agreement with the one dimensional and two dimensional periodic simulations. A mode cascade also occurs at the interface between the debris and the background plasma, leading to the longest wavelength possible at the end of the simulation in the debris plasma. Note, however, that now the debris-air interface is no longer sharp; debris ions have diffused upstream of the interface and exhibit strong variations in x. Because these debris ions have leaked out to where they can interact with waves produced at the shock, and because the IIF and the AIC instabilities have similar linear and nonlinear properties, the origin of the debris structure in this region is unclear. One also sees in the B_y plot that waves occur at the shock front and that the wavelength is not the longest possible for the simulation (i.e., no mode cascade). This is because the ion temperature anisotropy at the shock which drives the AIC instability is continually being maintained by reflected ions.

Other two dimensional nonperiodic simulations have been done varying the initial conditions, the system lengths, the Alfven Mach number, the thermal speeds, and the thickness of the debris piston. The general features of the simulations are largely independent of these parameters as long as $M_A \gg 1$, the directed velocity of the debris is much larger than the thermal speeds of the ions, and the system length includes relevant wave lengths. Figure 9 shows the results of another run (Case 8), with the same parameters as Case 7 (same debris mass and velocity) but with a much narrower piston initially ($10c/\omega_i$). Again, fluctuations due to the IIF are produced at early time before the shock forms, with amplitudes comparable to the previous case. (The waves in the debris look smaller because the maximum debris density is much larger). At later times there are again three regions: (1) waves at the shock front due to the IAC, (2) waves at the debris-air interface, which is not well separated yet from the shock, and (3) waves of smaller amplitude behind the debris slug in air that has already interacted with the debris via the IIF instability and has been left behind. At later times, remnant fluctuations from the shock will continue to interact with the shocked air, so that it is not possible to easily determine the origin of the late time structure.

Finally we note that the presence of the largest amplitudes at the interface explains why the initial conditions regarding the magnetic field penetration into the debris piston is largely irrelevant for the most significant structure. For realistic H.A.N.E. situations, the interface would be expected to be the most important for the early time structuring since the magnetic field will not have penetrated through the complete debris piston early in time. We again remark that it is largely irrelevant whether the debris is being controlled

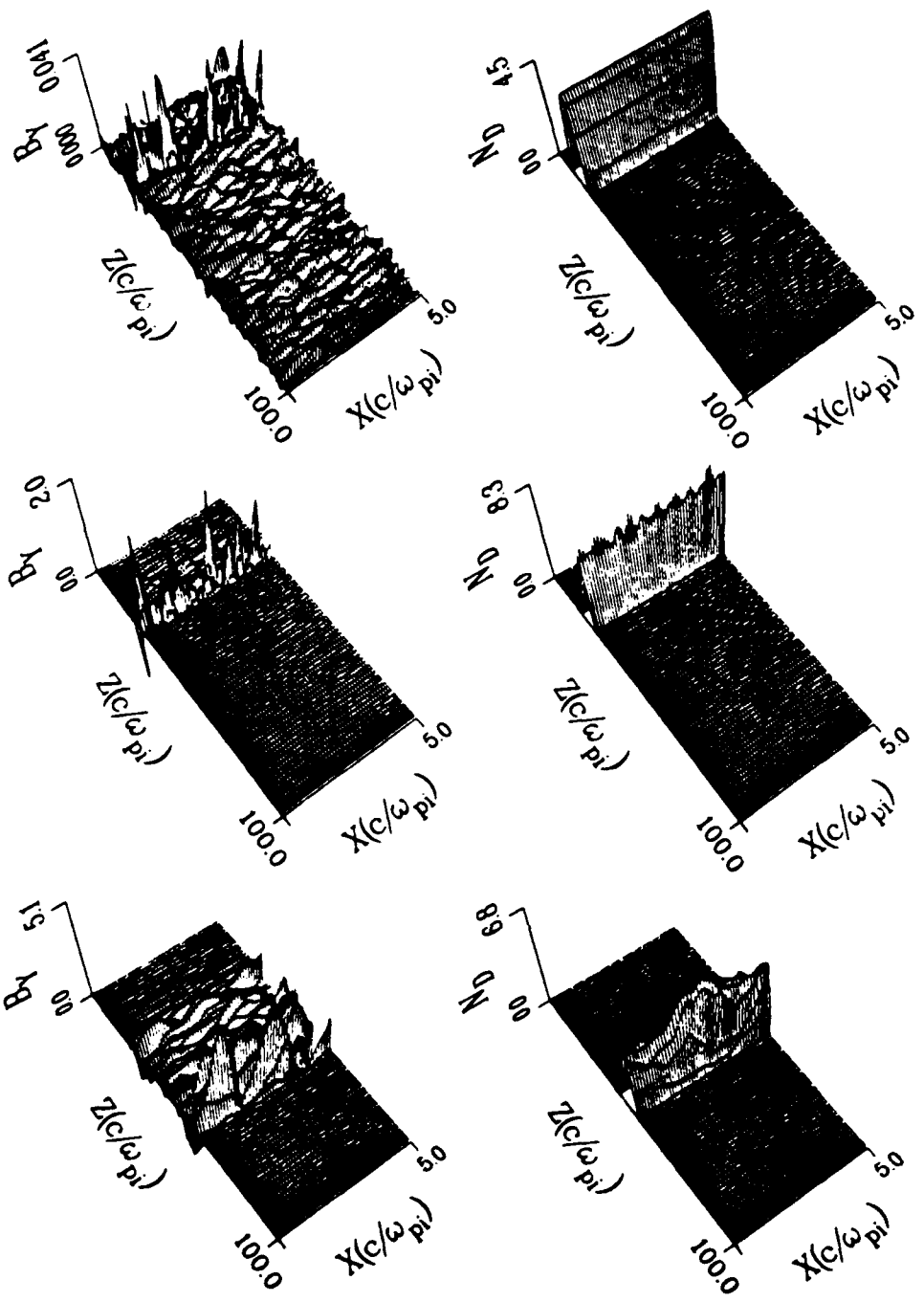

Figure 9. Same as Figure 8, but for a case with narrower debris initially, $L_D = 10c/\omega_i$. The perturbations in B_y at the shock front and in n_D at the debris-air interface are about the same magnitude, and smaller fluctuations persist in the air that has been left behind after interacting with the debris.

by one instability or the other; the important point is that the piston is structured on ion inertial length scales and remains so on an interestingly long time scale.

IV. Discussion

This report has demonstrated several properties of the ion-ion filamentation instability. Overall, the instability is very similar to the AIC instability caused by $T_{i\perp}/T_{i\parallel} \gg 1$, which is not surprising, as the ion-ion filamentation instability also is driven by an anisotropy, but due to relative ion streaming across a magnetic field. Both instabilities have similar growth characteristics, and both saturate at about the same levels in terms of field perturbations for a given free energy. Both instabilities evolve via a mode cascade, which involves short wavelength perturbations growing first and removing some of the anisotropy in the ion energy, followed by slower growing, long wavelength perturbations that dominate the long time, nonlinear behavior. It is during this later stage that the remaining ion energy anisotropy is removed.

A major difference in the two instabilities is that the ion-ion filamentation instability produces large amplitude density perturbations in a homogeneous system whereas the AIC instability does not. This is apparently due to the fact that the AIC distribution is assumed to be gyrotropic whereas the filamentation distribution function is not. None the less, it is useful to remember the strong connection between the two instabilities. One manifestation of this similarity is that in a nonuniform shock system both instabilities produce significant density structure of comparable amplitude and wavelength.

An important question relating to H.A.N.E.'s is whether the structure produced by the filamentation instability is long-lived. Periodic simulations show that the density structures cascade to long wavelengths where they remain for a long time. However, uniform periodic simulations are of questionable value for this particular effect, because in an isolated system there is no place for the energy to go. For this reason two dimensional simulations appropriate for shock formation were also performed. Simulations, initialized assuming either that the magnetic field is already diffused through the debris plasma, or alternatively that there was no magnetic field in the debris plasma initially, demonstrated rapid growth of the ion-ion filamentation instability on a time short compared to shock formation. The initial density perturbations persisted in a compressed and amplified form at the interface between the debris plasma and the background plasma, even after the shock wave itself was located far ahead of the debris air interface. However, because of the similar characteristics of the two modes, the simulations were not able to unambiguously determine whether the structure in the debris piston was associated more with the ion-ion filamentation instability which occurred before shock formation, or was a manifestation of the AIC instability taking place in the disturbed background plasma at the shock front. In addition, the largest fluctuations occur in the region of steep gradients at the

debris-air interface, suggesting strong coupling to other modes, such as the drift mirror and compressional drift modes [Migliuolo, 1983].

Other simulations of debris-air interactions have been carried out in recent years, but did not show the development of the IIF instability. Goodrich *et al.* [1985] did hybrid simulations of the initial debris-air coupling, but because the calculations were 1-D, with $\vec{B}$ (and thus $\vec{k}$ for the IIF) perpendicular to the simulation direction, the IIF could not have developed. Winske [1986] carried out particle simulations of debris-air interactions; in most of the runs the ions were unmagnetized, so again the IIF could not be excited. Even in cases with magnetized ions, however, the system size, chosen to resolve short wavelength electrostatic modes, was probably too small for proper growth of the IIF. Finally, Thomas and Brecht [1986] and Winske and Quest [1986] did 2-D hybrid simulations, similar to those described in Sec. III. In many of these cases the debris shell was very narrow ($\sim 10c/\omega_i$), and rather large spatial mesh ($\Delta \simeq 0.5c/\omega_i$) and time steps ($\Omega_i \Delta t \simeq 0.1$) were used to study the long time behavior of the shock that forms in the air. These again contributed to inhibit the growth of the IIF. While large fluctuations were observed at the debris-air interface on the time scale of the shock formation, they were attributed to the AIC, rather than the IIF instability. In the calculations of Thomas and Brecht [1986] any development of structure in the debris could not be followed in time, as the calculations were done in the shock frame, causing the debris ions to eventually leave the simulation region.

While the present simulations nicely illustrate structure development in the debris, we should also point out some limitations of the calculations. First, we have considered only cases where the magnetic field is exactly perpendicular to the streaming direction. As a consequence, the debris and air ions stay relatively isolated, which allows the best separation of effects due to the IIF and the AIC instabilities. In the more realistic case of oblique orientation of the magnetic field relative to the streaming direction, significant diffusion of the debris into the air occurs. Thus makes the distinction between the IIF and the AIC nearly impossible. Second, the simulations here were run for only about one gyroperiod, just long enough to observe the growth of the IIF instability and the formation of the leading shock wave. Clearly, to investigate the persistence of the debris structure the simulations will have to be run for much longer periods of time. Third, the two dimensional nature of the simulations imposes unphysical constraints. The conserved canonical momentum in the symmetry plane of the simulations prevents ions from moving more than about an ion gyroradius from the burst field line, and so there is no possibility for the macroscopic shock behavior to be affected by the debris clumps. In a real three dimensional system, this is no longer the case and the initial debris perturbations may have some effect on the shock front. For instance, the shock may produce jets of debris material in certain directions, depending upon the angular mass and velocity distribution of the debris piston. The debris clumps may also seed low Mach number structuring instabilities for those cases where the interaction changes quickly from high M_A to low M_A (e.g., upward expansion of the burst).

In conclusion, the simulations presented in this paper suggest that the ion-ion filamentation instability may generate some of the structured ionization in both the debris and the background plasma. Perturbations in the debris density much larger than the ambient density ($\delta n_D \gg n_A$) have been observed. However, it should be kept in mind that the largest waves occur at the debris-air interface, where they are enhanced by the strong gradients and perhaps by the computational constraint of 2-D and/or the initial conditions. The long time behavior should be dominated by waves of comparable amplitude and wavelengths on the order of $k_{\|}c/\omega_{pi} \sim 1$ Three dimensional calculations will be required to determine if the ion-ion filamentation instability has any global effect upon shock stability, and 2-D calculations run to much longer in time are needed to realistically determine whether this early time structure impacts the late time state.

Acknowledgements

We wish to thank Drs. S. H. Brecht and J. R. Thompson for useful discussions. This work was performed under the auspices of the U. S. Department of Energy and was supported by the Defense Nuclear Agency under Project Code RB, Task Code RC, Work Unit Code 167, and Work Unit Title separation "Simulations and Modeling of HANE/VHANE".

Appendix: Comparison of Ion-Ion Filamentation and Alfven Ion Cyclotron Instabilities for Debris Piston/Shock

We consider the situation depicted in Figure 1 in more detail. The debris is characterized by density n_D, mass m_D, velocity $V_D \perp B_o$, while the corresponding air quantities are n_A, m_A, and $V_A = 0$. In the regime where the debris overruns the air, the mean density, mass, and velocity are thus:

$$\bar{n} = n_A + n_D \tag{A.1}$$

$$\bar{m} = (n_A m_A + n_D m_D)/\bar{n} \tag{A.2}$$

$$\bar{V} = (n_D m_D V_D + n_A m_A V_A)/\bar{n}\bar{m} \tag{A.3}$$

Recalling that for both the AIC and IIF (Section 2):

$$\frac{\gamma}{\Omega_i} \simeq (\frac{\beta_i}{2}\frac{T_\perp}{T_\parallel})^{1/2} \tag{A.4}$$

$$\frac{kc}{\omega_i} \simeq \frac{3}{4}(\frac{T_\perp}{T_\parallel})^{1/2} \tag{A.5}$$

In the debris region, $T_\parallel = \frac{1}{2}\bar{n}\bar{m}v_i^2$, where v_i =thermal velocity (for simplicity the same for both species), while

$$T_\perp = \frac{1}{2}\bar{n}\bar{m}\bar{V}_\perp^2 = \frac{1}{2}n_A m_A(V_A - \bar{V})^2 + \frac{1}{2}n_D m_D(V_D - \bar{V})^2 \tag{A.6}$$

Normalizing to air quantities, $\Omega_A = eB_o/m_A c$, $\omega_A = (4\pi n_A e^2/m_A)^{1/2}$ and defining the Mach number $M_D = V_D/v_A$ (where $v_A^2 = B_o^2/4\pi n_A m_A$) and $\beta_A = 8\pi n_A T_\parallel/B_o^2$, one finds for the IIF:

$$\frac{\gamma}{\Omega_A} = \frac{1}{\sqrt{2}}\frac{(1+N)(NM)^{1/2}}{(1+NM)^{3/2}}M_D \tag{A.7}$$

$$\frac{kc}{\omega_A} = \frac{3}{4}\frac{(1+N)(NM)^{1/2}}{(1+NM)^{3/2}}\frac{M_D}{\beta_A^{1/2}} \tag{A.8}$$

where $N = n_D/n_A$, $M = m_D/m_A$. Taking $N \gg 1$ and $M \simeq 2$, this reduces to

$$\frac{\gamma}{\Omega_A} \simeq \frac{M_D}{2\sqrt{2}} \tag{A.9}$$

$$\frac{kc}{\omega_A} \simeq \frac{3}{8}\frac{M_D}{\beta_A^{1/2}} \tag{A.10}$$

In the shock region the debris is irrelevant; the AIC is driven by reflected ions, with density $n_r = \alpha n_A$ and velocity $V_r \sim V_D$, so that

$$nT_\perp \sim \frac{1}{2} n_r m_A \bar{V}_\perp^2 \sim \frac{\alpha}{2} n_A m_A V_D^2 \qquad (A.11)$$

Proceeding as before, we find for the AIC

$$\frac{\gamma}{\Omega_A} \simeq (\frac{\alpha}{2})^{1/2} M_D \qquad (A.12)$$

$$\frac{kc}{\omega_A} \simeq \frac{3\alpha^{1/2}}{4} \frac{M_D}{\beta_A^{1/2}} \qquad (A.13)$$

Because for high Mach number interactions $\alpha \rightarrow 1/3$ [Quest, 1986], it is evident from comparing (A.9-10) with (A.12-13) that the growth rates and wavenumbers of the two instabilities are indistinguishable.

References

Ambrosiano, J. and S. H. Brecht, A simulation study of the Alfven ion cyclotron instability in high beta plasmas, *Phys. Fluids, 30*, 108, 1987.

Brackbill, J. U., and D. W. Forslund, An implicit method for electromagnetic simulation in two dimensions, *J. Comput. Phys., 46*, 271, 1982.

Brecht, S. H., and V. A. Thomas, Multidimensional simulations using hybrid particle codes, *Comput. Phys. Comm., 48*, 135, 1988.

Davidson, R. C., and J. M. Ogden, Electromagnetic ion cyclotron instability driven by ion energy anisotropy in high beta plasmas, *Phys. Fluids, 18*, 1045, 1975.

Goodrich, C., K. Papadopoulos, and J. D. Huba, Early time coupling studies using a 1-D hybrid code, NRL Memo Report 5553, 1985.

Harned, D. S., Quasineutral hybrid simulations of macroscopic plasma phenomena, *J. Comp. Phys., 47*, 452, 1982.

Lampe, M., W. M. Manheimer, and K. Papadopoulos, Anomalous transport coefficients for HANE applications due to plasma microinstabilities, NRL Memo Report 3076, 1975.

Lemons, D. S., D. Winske, and S. P. Gary, Nonlinear theory of the Weibel instability, *J. Plasma Phys. 21*, 287, 1979.

Migliuolo, S., High beta theory of low frequency magnetic pulsations, *J. Geophys. Res., 88*, 2065, 1983.

Morse, R. L., and C. W. Nielson, Simulation of the Weibel instability, *Phys. Fluids, 14*, 830, 1971.

Otani, N. F., The Alfven ion-cyclotron instability: simulation theory and techniques, *J. Comp Phys. 87*, 251, 1988.

Quest, K. B., Simulations of high Mach number perpendicular shocks with resistive electrons, *J. Geophys. Res., 91*, 8805, 1986.

Quest, K. B., Hybrid simulations, *Proceedings of the Third School for Space Simulations*, La Londe Les Maures, France, 1988.

Tanaka, M., Simulations of heavy ion heating by electromagnetic ion cyclotron waves driven by proton temperature anisotropies, *J. Geophys. Res., 90*, 6459, 1985.

Tanaka, M., C. C. Goodrich, D. Winske, and K. Papadopoulos, A source of backstreaming ions in the foreshock region, *J. Geophys. Res., 88*, 3046, 1983.

Thomas, V. A., Dimensionality effects in hybrid simulations of high Mach number collisionless perpendicular shocks, *J. Geophys. Res.*, submitted, 1989.

Thomas, V. A., and S. H. Brecht, Two dimensional simulation of high Mach number plasma interactions, *Phys. Fluids, 29*, 2444, 1986.

Thompson, J. R., M. L. Sloan, G. I. Bourianoff, and B. N. Moore, The ion-ion filamentation instability, DNA-TR-88-97, 1988.

Winske, D., Microtheory and simulations for early time HANE: lower hybrid instabilities, Los Alamos Report LA UR 86-2292, 1986.

Winske, D., and K. B. Quest, Hybrid simulations of debris-air interactions: ions streaming perpendicular to the magnetic field, Los Alamos Report LA UR 86-4297, 1986.

Winske, D., and K. B. Quest, Magnetic field and density fluctuations at perpendicular supercritical collisionless shocks, *J. Geophys. Res., 93*, 9681, 1988.

Wu, C. S., D. Winske, Y. M. Zhou, S. T. Tsai, P. Rodriguez, M. Tanaka, K. Papadopoulos, K. Akimoto, C. S. Lin, M. M. Leroy, and C. C. Goodrich, Microinstabilities associated with a high Mach number perpendicular bow shock, *Space Sci. Rev., 37*, 63 1984.

DISTRIBUTION

Dr. B. H. Ripin
Code 4732
Naval Res. Lab.
Washington, DC 20375

Dr. E. McLean
Code 4732
Naval Res. Lab.
Washington, DC 20375

Dr. J. Stamper
Code 4732
Naval Res. Lab.
Washington, DC 20375

Dr. Paul Bernhardt
Code 4780
Naval Res. Lab.
Washington, DC 20375

Dr. Walter Chesnut
SRI International
333 Ravenswood Ave.
Menlo Park, CA 94025

Dr. J. L. Sperling
JAYCOR
11011 Torreyana Road
P. O. Box 85154
San Diego, CA 92138

Dr. R. Stellingwerf
Mission Research Corp.
1720 Randolph Rd. S. E.
Albuquerque, NM 87106

Dr. R. Peterkin
Mission Research Corp.
1720 Randolph Rd. S. E.
Albuquerque, NM 87106

Dr. K. Hain
Maxwell S-Cubed Div.
1800 Diagonal Rd.
Alexandria, VA 22314

Dr. E. Hyman
SAIC
1710 Goodridge Dr.
McLean, VA 22102

Dr. J. Guillory
PRC
5850 Leesburg Pike # 23
Falls Church, VA 22041

Dr. L. Wittwer
RAAE
Defense Nuclear Agency
Washington, DC 20305

Dr. B. Prasad
RAAE
Defense Nuclear Agency
Washington, DC 20305

Director [2]
Attn: STTI
Defense Nuclear Agency
Washington, DC 20305-1000

Dr. R. W. Kilb
Mission Research Corp.
P. O. Box 719
Santa Barbara, CA 93102

Dr. W. W. White
Mission Research Corp.
P. O. Box 719
Santa Barbara, CA 93102

Dr. M. Hausman
Mission Research Corp.
P. O. Box 719
Santa Barbara, CA 93102

Dr. D. Sowle
Mission Research Corp.
P. O. Box 719
Santa Barbara, CA 93102

Prof. D. Papadopoulos
Astronomy Program
University of Maryland
College Park, MD 20742

Dr. J. D. Huba
Code 4780
Naval Res. Lab.
Washington, DC 20375

Dr. J. Lyon
Code 4780
Naval Res. Lab.
Washington, DC 20375

Dr. J. Giuliani
Code 4780
Naval Res. Lab.
Washington, DC 20375

Dr. S. Brecht
Berkeley Research Associates
P.O. Box 241
Berkeley, CA 94701

Dr. V. Thomas
Berkeley Research Associates
P.O. Box 241
Berkeley, CA 94701

Dr. H. Carl Fitz
Physical Research, Inc.
134 Holiday Ct., Suite 309
Annapolis, MD 21401

Dr. R. Armstrong
Mission Research Corp.
One Tara Blvd. Suite 302
Nashua, NH 03062

Defense Technical Information Center [2]
Cameron Station
Alexandrai, VA 22314

Dr. R. Henderson, W385
Director, JASON Program Office
The MITRE Corp.
7525 Colshire Dr.
McLeam, VA 22102

DASIAC
815 State St.
P.O. Drawer QQ
Santa Barbara, CA 93102

Dr. J. Kindel
MRC
127 Eastgate #20800
Los Alamos, NM 87544

Dr. T. Mazurek
Mission Research Corp.
P. O. Box 719
Santa Barbara, CA 93102

Dr. C. Longmire
Mission Research Corp.
P. O. Box 719
Santa Barbara, CA 93102

Dr. E. Witt
Mission Research Corp.
P. O. Box 719
Santa Barbara, CA 93102

Dr. J. R. Thompson
Austin Research Associates
1901 Rutland Dr.
Austin, TX 78758

Dr. J. M. Cornwall
Dept. of Physics
UCLA
Los Angeles, CA 90024

Dr. D. Hammer
Laboratory for Plasma Studies
809 Upson Hall
Cornell University
Ithaca, NY 14853

Dr. C. Prettie
Berkeley Research Associates
P.O. Box 241
Berkeley, CA 94701

Dr. J. Workman
Berkeley Research Associates
P.O. Box 241
Berkeley, CA 94701

Dr. D. Simons
ESS-7
MS D466

Dr. D. Sappenfield
ESS-7
MS D466

Dr. G. Smith
ESS-DOT
MS D446

Dr. M. Pongratz
ESS-DOT
MS D446